Hadamard Encoding of 2D-Selective RF Excitations for Simultaneous Acquisition of Multiple, Irregularly Shaped Voxel in MR Spectroscopy

M. G. Busch[1,2], and J. Finsterbusch[1,2]

[1]Department of Systems Neuroscience, University Medical Center Hamburg-Eppendorf, Hamburg, Germany, [2]Neuroimage Nord, University Medical Centers Hamburg-Kiel-Lübeck, Hamburg-Kiel-Lübeck, Germany

Introduction

2D-selective RF (2DRF) [1,2] excitations have been used to acquire single voxel MR spectra of irregularly shaped target regions [3,4] which, compared to conventional localization based on cross-sectional RF excitations, reduces partial volume effects. In this study, it is shown that the SNR efficiency of such approaches can be increased by acquiring multiple, irregularly shaped voxel simultaneously and applying Hadamard encoding [5-7] to eliminate the individual contributions.

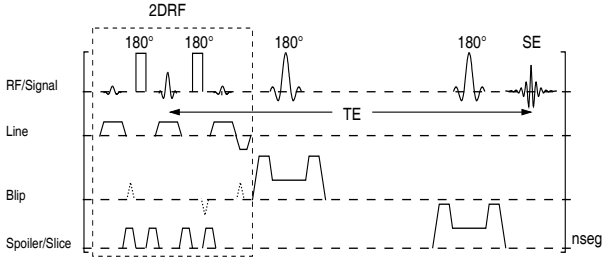

Fig. 1: Basic PRESS pulse sequence for MRS spectroscopy of irregularly shaped voxel using segmented blipped-planar 2DRF excitations. The shown three-line segment covers the central k-space line, the other segments are shifted in the blip direction which requires adapting the gradient blips and their rephasing gradients (dotted) accordingly taking the non-selective refocusing RF pulses into account.

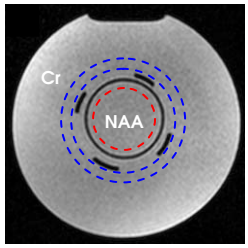

Fig. 2: MR image of the two-bottle phantom containing NAA in the inner and creatine in the outer bottle: The dashed lines indicate the ring (blue) and circle profile (red) used.

Methods

A PRESS-based pulse sequence was used as shown in Fig. 1. As the initial RF excitation a 2DRF excitation based on a segmented blipped-planar trajectory was used. The desired excitation profile then is obtained by complex averaging all acquired signals. Non-selective refocusing RF pulses were applied between the individual 2DRF lines to avoid chemical-shift-displacement artifacts in the blip direction. The first selective refocusing RF pulse was applied in the blip direction and was used to eliminate the (unwanted) side excitations, which allows reducing the field-of-excitation and the number of 2DRF lines accordingly. A fast-spin-echo variant of the sequence with phase- and frequency-encoding gradients added in the line-blip plane was implemented to measure images of the 2DRF excitation profiles.

The 2DRF pulse envelope was calculated using the low-flip-angle approximation [2] by taking the Fourier transformation of the desired excitation profile. Four acquisitions were performed for each combination of two ROIs using different signs for the individual ROIs in the excitation profile (+/+, +/–, –/+, –/–) where "–" indicates that the corresponding signal phase was inverted by applying an appropriate modulation of the RF envelope. The individual contributions were obtained by adding and subtracting the acquisitions accordingly. Two setups were investigated: (i) a ring- and a circle-shaped ROI which were used to demonstrate the elimination of the individual spectral contributions in a dedicated MR spectroscopy phantom (see Fig 2), and (ii) two irregularly shaped ROIs (resolution of 1×1 mm^2) that were defined on a high-resolution T1-weighted data set of a healthy volunteer and covered gray and white matter, respectively (see Fig. 5a).

Experiments were performed on a 3 T whole-body MR system (Siemens Magnetom Trio) using a 12-channel head coil. An oil phantom (profile images) and a dedicated spectroscopy phantom (MR spectra) consisting of a small bottle containing aqueous NAA solution that is positioned within a larger bottle filled with aqueous creatine solution (see Fig. 2) were investigated. 2DRF excitations were applied with a resolution of 1×1 mm^2, a field-of-excitation of 80 mm, and 16 segments, each covering 5 lines, yielding a 2DRF pulse duration of 28 ms. MRS acquisitions involved 6 averages (10 min total acquisition time), an echo time of 60 ms, a voxel thickness of 10 mm, four preparation scans, and three CHESS pulses for water saturation. Profile images were acquired with a TR of 6 s, a TE of 80 ms, and an in-plane resolution of 1×1 mm^2, and stored as real part and phase images to retain the sign and phase of the profile.

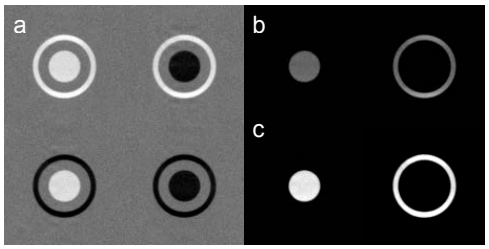

Fig. 3: (a) Real part MR images of the ring/circle ROIs acquired with the four polarity combinations. (b,c) Sum/difference images of (a) to eliminate the circle and ring contributions by using (b) only the upper two real images and (c) all four images.

Results and Discussion

Figure 3 presents profile acquisitions for the ring-circle ROI combination and the sum / difference images to eliminate the ring and circle contributions, respectively. Using all four combinations acquired yields a better signal amplitude (Fig. 3c) due to the effectively longer acquisition time, but for a proper elimination of the ring and circle profiles it is sufficient to use two acquisitions only (Fig. 3b). This can be verified in the corresponding MR spectra (Fig. 4) that also demonstrate the higher signal amplitude achieved with the Hadamard-encoded acquisitions compared to the simple acquisition that would be required for the ring and circle profile individually. Figure 5 shows results obtained for the WM/GM ROIs which also can be isolated clearly.

When defining the multiple ROIs, it is recommended to leave a small gap between them. Thus, variations of the slope between the ROIs upon a change of the polarity are avoided.

In conclusion, Hadamard-encoding may help to improve the SNR efficiency of MRS acquisitions with irregularly shaped voxels.

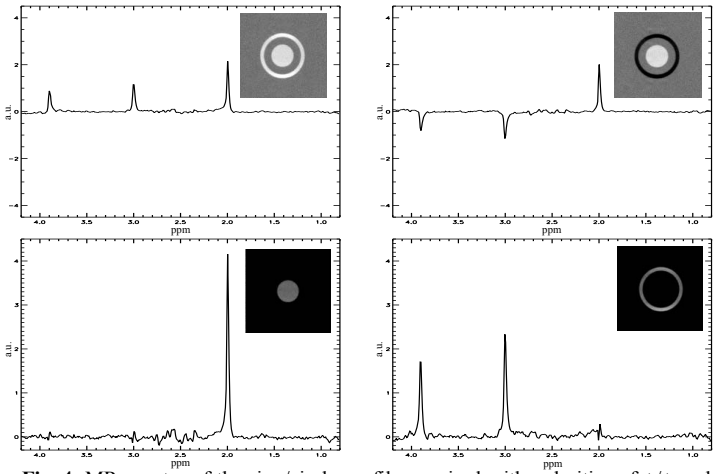

Fig. 4: MR spectra of the ring/circle profile acquired with polarities of +/+ and +/–, respectively (upper) and sum and difference spectra yielding the metabolite signals present in the circle (NAA, left) and the ring profile (creatine, right).

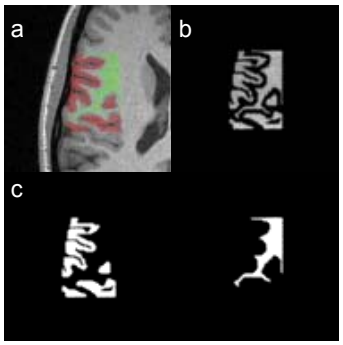

Fig. 5: (a) WM/GM ROIs (green/red) defined using the underlying T1-weighted image of a healthy volunteer. (b) Real part profile image of the WM/GM ROI (both with positive polarity) and (c) sum and difference images of two acquisitions (++/+–) to eliminate one of the contributions.

References

[1] Bottomley PA, Appl Phys 62, 4284 (1987)
[2] Pauly J, J Magn Reson 81, 43 (1989)
[3] Qin Q, Magn Reson Med 58, 19 (2007)
[4] Weber-Fahr W, Magn Reson Imaging 27, 664 (2009)
[5] Dreher W, Magn Reson Med 31, 596 (1994)
[6] Doan BT, J Magn Reson 198, 94 (2009)
[7] Börnert P, MAGMA 16, 86 (2003)